Available online at www.sciencedirect.com
SCIENCE DIRECT®
ELSEVIER
European Journal of Mechanics B/Fluids 23 (2004) 41–49
EUROPEAN JOURNAL OF MECHANICS B/FLUIDS

Predictability and uncertainty in flow–structure interactions

Didier Lucor, George Em Karniadakis *

Center for Fluid Mechanics, Division of Applied Mathematics, Brown University, 182 George Street, Providence, RI 02912, USA

Received 28 February 2003; accepted 15 May 2003

Abstract

Direct numerical simulation advances in the field of flow–structure interactions are reviewed both from a deterministic and stochastic point of view. First, results of complex wake flows resulting from vibrating cylindrical bluff bodies in linear and exponential sheared flows are presented. On the structural side, non-linear modeling of cable structures with variable tension is derived and applied to the problem of a catenary riser of complex shape. Finally, a direct approach using Polynomial Chaos to modeling uncertainty associated with flow–structure interaction is also described. The method is applied to the two-dimensional flow–structure interaction case of an elastically mounted cylinder with random structural parameters subject to vortex-induced vibrations.

Keywords: Flow–structure interactions; Sheared flows; Non-linear cables; Uncertainty; Polynomial chaos

1. Introduction

Prediction of vortex induced vibrations (VIV) has been a semi-empirical discipline until recently. Most of the models employed in industrial applications (e.g., SHEAR7, VIVA, etc.) involve eigensolutions of the structure but the required flow input (e.g., lift coefficients, added mass, correlation length, etc.) is obtained empirically.

In the mid-1990s we initiated a research program in Direct Numerical Simulation (DNS) of three-dimensional general flow–structure interactions in order to fill this gap. Our main focus has been on simulating VIV for flows past cylindrical flexible structures. We started at low Reynolds number (of the order of 100 to 200) and relatively small aspect ratio (of the order of 10). However, today based on new algorithms and faster parallel processors we simulate VIV at Reynolds number of the order of a few thousands and flexible cylinders of aspect ratio of the order of 1000. Although this range is still below the Reynolds numbers of industrial applications, from this new range extrapolations can be made, and indeed most of the predictions agree with experimental measurements quantitatively. Progress has also been made with respect to the type of structures we can simulate. Our initial efforts involved linear structures but more recent work has focused on non-linear structures with sag and vibrations in all three direction, i.e., including the axial direction.

In this paper, we present some highlights of our work with emphasis on sheared inflow and non-linear structures. We also present our new path of research that attempts to model from first principles the various uncertainties associated with flow–structure interaction problems. This leads to a coupled system of stochastic differential equations for the flow and the structure, a computationally prohibitive task at first glance. However, we present a new approach to model stochasticity that involves extensions to the *polynomial chaos* method pioneered by Norbert Wiener in the late 1930s. The generalization of this approach could lead to a new generation of *non-sterilized* simulations of VIV, where uncertainties in flow conditions, structural properties and support are modeled explicitly.

* Corresponding author.
E-mail addresses: didi@dam.brown.edu (D. Lucor), gk@cfm.brown.edu (G.E. Karniadakis).

0997-7546/$ – see front matter
doi:10.1016/j.euromechflu.2003.05.001

2. VIV of flexible cylinders with sheared inflow

Following the work in [1,2] of Direct Numerical Simulations (DNS) of uniform inflow past flexible cylinders subject to Vortex Induced Vibrations (VIV), we have focused on the physics of more complex flows corresponding to a wide range of inflow conditions. In particular, we have investigated different sheared (*linear* or *exponential*) inflows past medium and long free flexible cylinders (aspect ratio from around 20 diameters to more than 1000 diameters). We have also investigated oblique inflows with large angle of yaw past free rigid cylinders to access the validity of the *Independence Principle* [3].

In the simulations, we employ the parallel three-dimensional version of the $\mathcal{N}\varepsilon\kappa\mathcal{T}\alpha r$ code with a linear model for the structure and a Fourier expansion with a 3/2 de-aliasing rule in the longitudinal cable direction. We only consider crossflow motion of the structure which is described by the following equation:

$$\frac{\partial^2 Y}{\partial t^2} - c^2 \frac{\partial^2 Y}{\partial z^2} + \gamma^2 \frac{\partial^4 Y}{\partial z^4} + \frac{4\pi\zeta}{U_r}\frac{\partial Y}{\partial t} + \left(\frac{2\pi}{U_r}\right)^2 Y = \frac{1}{2}\frac{C_L}{m}, \tag{1}$$

where we denote by $Y(z,t)$ the non-dimensional cross-flow displacement, that has been normalized by the cylinder diameter d. The damping fraction is ζ and $U_r = U/fd$ is the reduced velocity. The mass ratio is m and f is the natural frequency of the structure. The maximum shear inflow velocity is taken as the reference velocity U for the system. The coefficient C_L is the total lift force, i.e., including both pressure and viscous contributions. Also, $c = \sqrt{T/\rho_s U^2}$ and $\gamma = \sqrt{EI/\rho_s U^2 d^2}$ (where ρ_s is the structural linear density) are the non-dimensional cable and beam phase velocity respectively, where T is the tension and EI is the bending stiffness. The lift force is obtained through the flow solver.

A boundary-fitted coordinate system is employed similar to the simulations in [4], which has been validated against an Arbitrary Lagrangian Euler (ALE) formulation [5]. The aforementioned approach is preferred for long flexible risers as it provides a very efficient way to solve for the structure. The Fourier modal decomposition of the linear structural response is very convenient in this case. Moreover, a general full three-dimensional mesh for large aspect ratio is prohibitively expensive; therefore, the spanwise Fourier decomposition offers a more flexible alternative and allows for a relatively low computational cost for solving for the flow.

Fig. 1 (right) shows an example of a linear sheared flow past a long flexible cylinder. Here the aspect ratio is $L/d = 567$ and the shear parameter is $\beta = (d/U)(\partial u/\partial z) = 8.82 \times 10^{-4}$, where z denotes the spanwise (cylinder axis) direction, d is the cylinder diameter, and U the span-averaged freestream velocity. We observe some vortex dislocations and vortex splits very similar to the ones obtained in [6] (see Fig. 1: left). Strong vortex dislocations can result in substantial modulation of the forces on the body as it has been documented in [7].

In Fig. 2 (right), we present another example of complex flow physics successfully captured by DNS. In this case, we properly resolve a vortex split that connects two vortical patterns ("$2S$" and "$2P$") along a rigid cylinder forced to move in the cross-flow direction with a prescribed amplitude and frequency, see also [8]. In contrast to vortex dislocations, this *hybrid* mode is periodic and repeatable with the location of the vortex split remaining stable.

Currents in the ocean are invariably highly sheared, hence the modes that can potentially be excited are many, see [9]. The calculation of *how many* and *which modes* are excited, can affect fatigue life very significantly. Obviously, spatial resolution in the spanwise direction becomes a critical issue for the modal prediction of the response. A sufficient number of Fourier modes have to be used in this direction in order to capture the scale of the correlation length of the flow.

We present a third case that corresponds to a cylinder with very large aspect ratio ($\geqslant$1500) subject to an *exponential shear* inflow described by an exponential distribution with long tail (see the inflow velocity profile in Fig. 3 left) where we vary the spanwise numerical resolution. We test 64 complex Fourier modes (Case 0-a) and 32 Fourier modes (Case 0-b) along

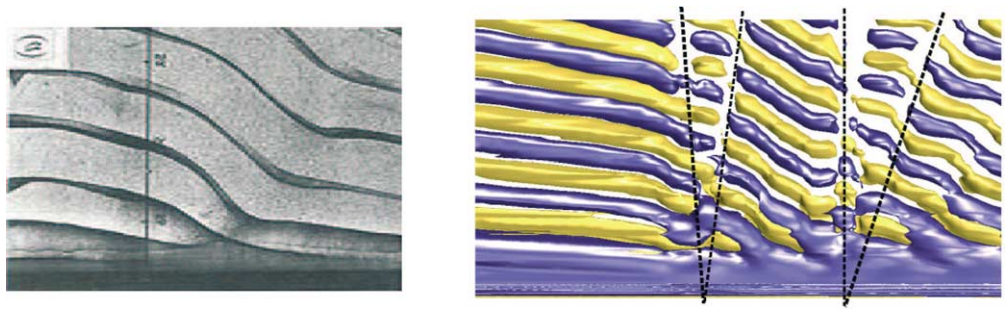

Fig. 1. Experimental (left) vs numerical (right) results. Left: photograph of vortex dislocation at $Re = 100$ for stationary cylinder using dye flow visualization (courtesy of Williamson [6]). Right: isocontours of spanwise vorticity ($\omega_z = \pm 0.18$) and oblique fronts in the wake of a forced vibrating flexible cylinder at $Re = 100$ with linear sheared inflow.

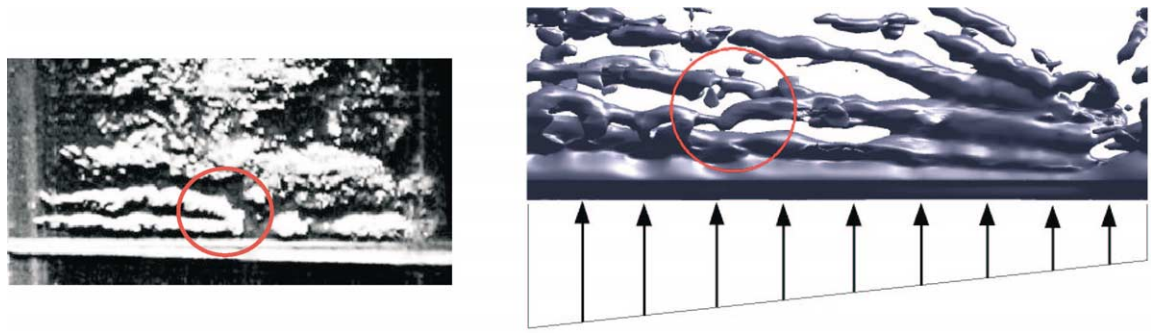

Fig. 2. Experimental (left) vs numerical (right) results. Left: photograph of vortex *split* in the wake of a forced rigid tapered cylinder at $Re_{\bar{d}} = 400$ with uniform inflow using lead precipitation visualization (courtesy of Techet et al. [8]). Right: isocontour of pressure ($p = -0.25$) in the wake of a forced rigid straight cylinder at $Re_{\overline{U}} = 400$ with *linear* sheared inflow.

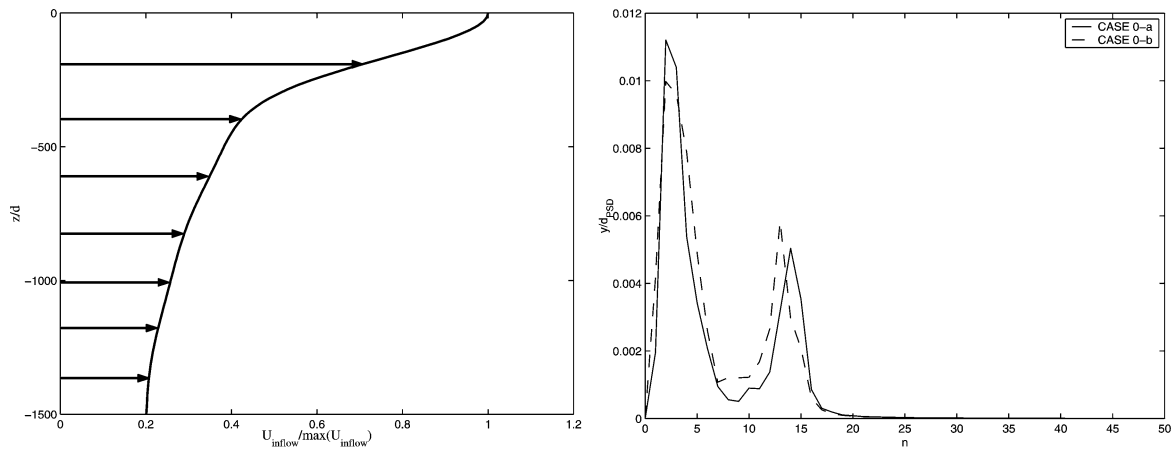

Fig. 3. Normalized inflow velocity profile (left). Time averaged power spectral density of cylinder crossflow displacement versus modes number n (right). Case 0-a: 64 Fourier modes; Case 0-b: 32 Fourier modes.

the spanwise direction. The initial conditions for Case 0-a and Case 0-b are identical. Moreover, we present the simulation results over a spanwise domain of interest corresponding to $L/d = 1500$ which is smaller than the computational domain. The computational domain extent is $L/d = 1844$ and the inflow velocity along the range which is not included in the results is constant and equal to its minimum value $U = 0.2$. The flexible beam-cable structure is pinned at both ends. The maximum Reynolds number is $Re = 1000$ and thus a turbulent near-wake is developed on the side of the high inflow. For this case, the corresponding eigenspectrum is determined by:

$$\omega^2 = \gamma^2 \left(\frac{n\pi}{L/d} \right)^4 + c^2 \left(\frac{n\pi}{L/d} \right)^2, \tag{2}$$

where n is the mode number. A lock-in phenomenon can occur if the structure's natural frequency is close enough to the Strouhal frequency of the flow. An estimate of the dominant modal response can be derived from the previous formula.

We obtain a *mixed response* for both cases, with coexistence of *standing* and *traveling* waves. Amplitude and velocity of the traveling waves for Case 0-b seem to cover a wider range and they fluctuate more than Case 0-a. Concerning the modal response of the structure, we see from Fig. 3 (right), that in addition to the low modes, it is mainly mode number $n = 14$ for Case 0-a and $n = 13$ for Case 0-b, which are excited in terms of oscillations of the structure around its mean position. In conclusion, low modes and low oscillation frequencies are not affected by the Fourier spanwise resolution. However, a decrease in the spanwise resolution causes a slight shift of the high modal response as well as of the structural Strouhal frequency to lower values. This could be explained by a change in the frequency and spanwise correlation of the hydrodynamical forces acting on the body. A coarser resolution in the spanwise direction could induce a stronger spanwise correlation of the lift forces and subsequently would induce a lower oscillation frequency in time.

The presence of strong low modes in the structural response of Case 0 seems to indicate that this feature is very sensitive to the magnitude of the inflow velocity on the side of the low inflow. However, other simulations (not presented here) with similar low inflow velocity but different initial conditions for the structure and for the flow did not produce any structural low modes response. In conclusion, it seems that the excitation of low modes can be sustained by the system for a long time if they are present in the initial condition.

3. Flow-induced vibrations of non-linear cables

Our next objective has been to bridge the gap that exists between studies of non-linear dynamic models for *general type* cables and DNS of flow past *simple* string/beam models. The former typically assumes a simplistic or empirical representation of excitation forces but provides very accurate models for the non-linear dynamic response of the cable allowing realistic description of both steel cables and synthetic cables with non-linear tension-strain relationship. The latter, on the other hand, assumes simple string/beam linear models but provides an accurate description of pressure and viscous forces, albeit (at present) in the low Reynolds number regime.

To this end, we have derived appropriate governing equations for non-linear cables and have developed a new formulation for the coupled flow–structure problem, see [10]. The structure is discretized using an explicit finite difference scheme with second-order accuracy in time and space while the flow is discretized using spectral/hp elements in the context of the arbitrary Lagrangian–Eulerian formulation (ALE). We have used effectively this new model to simulate large-scale industrial systems such as the lazy wave steel catenary riser (LWSCR), see below and also in [11].

3.1. Governing equations for non-linear cables

For *non-linear* cable, all three-directions are coupled and thus oscillations are excited both along the longitudinal (cable axis) direction as well as along the two transverse directions. We derive a unified formulation for non-linear cables in terms of a non-dimensional stretching parameter Δ.

Let us consider an infinitesimal segment of a stretched string in a "reference" position, which may not be in an equilibrium position. Let the arc length of the segment in this reference position be $\mathrm{d}S$. We parameterize our string with respect to the arc length variable in the reference position, so that at any time t, we have arc length parameter $s(S,t)$ and an infinitesimal segment of length $\mathrm{d}s(S,t)$. Let x, y and z be the two transverse and the longitudinal direction respectively, in an orthonormal coordinate frame for the string, then

$$\mathrm{d}s^2 = \mathrm{d}x^2 + \mathrm{d}y^2 + \mathrm{d}z^2 \Rightarrow \Delta = \frac{\partial s}{\partial S} = \sqrt{\left(\frac{\partial x}{\partial S}\right)^2 + \left(\frac{\partial y}{\partial S}\right)^2 + \left(\frac{\partial z}{\partial S}\right)^2}, \tag{3}$$

where Δ represents the length increase or decrease with respect to the reference position.

Let the tension in the string be $T(x,y,z)$ or $T(S,t)$ in terms of our fundamental parameterization. T is tangential to the string at all points, we refer to the external forces in the three coordinate directions as $\boldsymbol{F} = F_{x|y|z}$ and the position vector $\boldsymbol{X} = [x\ y\ z]^{\mathrm{T}}$.

The linear density of the string is $m_v(s,t)$-conservation of mass for the line segment demands that:

$$m_v(s,t)\,\mathrm{d}s = m_0(S_0)\,\mathrm{d}S_0 = m(S)\,\mathrm{d}S. \tag{4}$$

Given structural damping forces proportional to the string velocity (by a constant R), the fully non-linear equations are:

$$\frac{\partial}{\partial S}\left(\frac{T}{\Delta}\frac{\partial \boldsymbol{X}}{\partial S}\right) + \Delta\left[\boldsymbol{F}(S,t) - R\frac{\partial \boldsymbol{X}}{\partial t}\right] = m(S)\frac{\partial^2 \boldsymbol{X}}{\partial t^2}. \tag{5}$$

In the context of flow–structure interactions, F_x is drag, F_y is lift possibly with a gravitational body force $-m(S)g$, and F_z is the spanwise hydrodynamic force component.

The model for the tension derived for Poisson's ratio $P = 1/2$ can be written as:

$$T(s,t) = T(S) + EA(S)\left(1 - \frac{1}{\Delta}\right) = T_r + EA_r\left(1 - \frac{1}{\Delta}\right), \tag{6}$$

where $T(s,t)$ is expressed in terms of the tension in the reference position $T(S)$ and of a stretching term $EA(S)(1 - 1/\Delta)$. When the reference position is that of a straight stretched (uniform in radius) string, we can rewrite the equation (see third part of Eq. (6)) where both the tension in the reference position $T_r = EA_r\varepsilon$ and the cross-sectional area in the reference position A_r are constant.

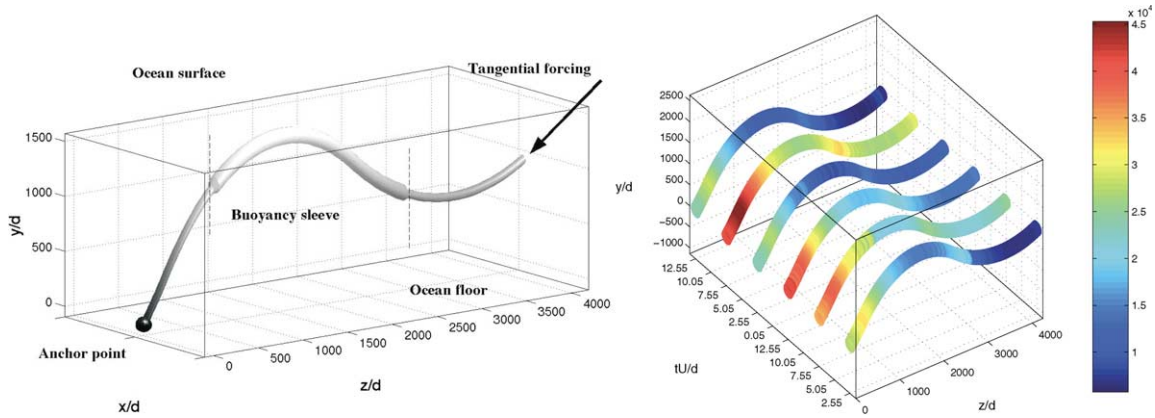

Fig. 4. Left: LWSCR static configuration schematic (sag-bend part with enlarged body diameter). Right: distribution of tension along the LWSCR sag-bend part at different times.

For the case of $P = 0$, the model for the tension takes the form:

$$T(s,t) = EA_0\big(\Delta\big(\varepsilon(S)+1\big)-1\big) = \Delta\left[T_r + EA_r\left(1-\frac{1}{\Delta}\right)\right], \tag{7}$$

where the last equality in the above equation is valid in the case of a reference position being a straight stretched string with uniform radius. It is worth mentioning that the presence or not of the incompressibility assumption leads to two different models for the tension, i.e., Eqs. (6) and (7) and a dependence of a different nature on the non-linear parameter Δ. This is relevant given that the assumption that changes in cross-sectional area are negligible is not that uncommon.

Details of the Arbitrary Lagrangian Eulerian (ALE) formulation that we use to solve for the flow in a moving domain with moving boundaries can be found in [12,5].

3.2. Flow induced vibration of a lazy wave riser

We consider a problem involving a riser of complex shape, which is immersed in quiescent flow. Specifically, we simulate the sag-bend response of the so-called lazy wave steel catenary riser (LWSCR) subject to a tangential forced motion at one end. The objective is to determine if the LWSCR in the absence of ocean current will experience intermittent flow-induced vibrations, and whether the resulting hydro-elastic excitation consists of a standing or a traveling wave response.

Fig. 4 (left) provides a 3D schematic of the lower part of the LWSCR static configuration with its buoyant sleeve. The structural model that we use accounts for time- and space-dependent tension in the structure. It also accounts for variable linear density of the structure. We use the tension model corresponding to Poisson ratio $P = 1/2$ (see Eq. (6)) and the tension of the structure in the reference position is taken constant, and thus we have $T(S) = T_0$. The reference position is, in this case, a straight stretched cable with constant tension. However, the code has the capability to treat a case with variable reference tension $T(S)$.

Fig. 4 (right) shows the *variable tension* in the structure. The plot shows six different configurations (corresponding to six different instants of time) and the corresponding magnitude of the tension is superimposed on the structure shape. The variation of tension, which is substantial, is larger in time than in space.

4. Modeling uncertainty

For flow–structure interactions the interest on stochastic modeling so far has primarily been on the dynamics of lumped systems, i.e., single- or two-degree-of-freedom second-order oscillators. The effect of the flow has been modeled via an interaction source term as either white noise or as a Gaussian distribution. However, non-Gaussian distribution behavior for the response has been documented in experiments. Here, we apply Wiener–Askey Polynomial Chaos method to solve stochastic coupled Navier–Stokes/structure system such as cylinders with random properties/boundary conditions subject to VIV.

The Wiener–Askey Polynomial Chaos expansion is a generalization of the original Polynomial Chaos. It is well suited to represent second-order random processes in terms of orthogonal polynomials. The expansion basis $\Psi_j(\boldsymbol{\xi}(\theta))$ is the complete

polynomial basis from the Askey-scheme [13]. Using this type of representation, a general second-order random process takes the form:

$$u(\boldsymbol{x},t;\theta)=\sum_{j=0}^{P}\hat{u}_j(\boldsymbol{x},t)\Psi_j\big(\boldsymbol{\xi}(\theta)\big)\quad\text{with } P=\frac{(n+p)!}{n!p!}-1, \tag{8}$$

where we typically truncate the series up to $P+1$ terms and where n is the number of random dimensions and p is the highest polynomial order of the Polynomial Chaos expansion. The vector $\boldsymbol{\xi}(\theta)$ is the vector of independent random variables ξ_i, functions of the independent random variable θ. Since each type of polynomials from the Askey-scheme forms a complete basis in the Hilbert space determined by their corresponding support, we can expect each type of Wiener–Askey expansion to converge to any L_2 functional in the L_2 sense in the corresponding Hilbert functional space as a generalized result of Cameron–Martin theorem. The numerical procedure can be greatly simplified as most of the orthogonal polynomials from the Askey-scheme have weighting functions that take the form of probability function of certain types of random distributions.

4.1. Incompressible Navier–Stokes equations

We consider incompressible flow which can behave randomly subject to the randomness imposed by boundary conditions or random forcing:

$$\nabla\cdot\mathbf{u}=0, \tag{9}$$

$$\frac{\partial\mathbf{u}}{\partial t}+\mathbf{u}\cdot\nabla\mathbf{u}=-\nabla\Pi+Re^{-1}\nabla^2\mathbf{u}. \tag{10}$$

We expand the velocity and pressure in terms of the Polynomial Chaos expansion (see Eq. (8)), i.e.,

$$\mathbf{u}(\boldsymbol{x},t,\theta)=\sum_{i=0}^{P}\boldsymbol{u}_i(\boldsymbol{x},t)\Psi_i\big(\boldsymbol{\xi}(\theta)\big), \tag{11}$$

$$\Pi(\boldsymbol{x},t;\theta)=\sum_{i=0}^{P}\Pi_i(\boldsymbol{x},t)\Psi_i\big(\boldsymbol{\xi}(\theta)\big). \tag{12}$$

We then substitute into the Navier–Stokes equations, and subsequently we project the obtained equations onto the random space spanned by the polynomial chaos basis. That is, we take the inner product with each basis and use the orthogonality condition to simplify the equations. We obtain a discrete set of deterministic equations for the random modes. The random modes are only coupled through the convective terms.

4.2. Application to flow–structure interactions

We consider the two-dimensional flow–structure interaction case of an elastically mounted circular cylinder with random structural parameters, subject to vortex-induced vibrations. We study the case of an unsteady flow in the laminar regime. The flow is computed using the procedure outlined above while the structural response (Eq. (13)) of the moving cylinder is computed using a very similar procedure described in [14]. For the temporal discretization we use the implicit second-order Newmark scheme [14] for the equation

$$\ddot{\eta}(t,\theta)+c(\theta)\dot{\eta}(t,\theta)+k(\theta)\eta(t,\theta)=\boldsymbol{F}(t,\theta),\quad \eta(0)=\eta_0\text{ and }\dot{\eta}(0)=\dot{\eta}_0. \tag{13}$$

We assume that the damping coefficient $c(\theta)$ and the spring factor $k(\theta)$ of the structure are both random variables. The free structure is excited by the vortex shedding of the flow and it follows a random response. Therefore, the position of the boundary of the cylinder becomes stochastic. This random boundary affects the flow domain, and consequently the flow itself becomes a stochastic process. The fluid forces on the cylinder are derived from the random flow velocity field and the random pressure field at every time step. To simplify the solution of the flow equations, we consider the initial coordinate system (x',y',t') and a coordinate system (x,y,t) attached to the moving cylinder. The stochastic flow equations are solved using a mapping approach based on the original deterministic mapping developed in [4]. This process maps the time-dependent and moving problem to a stationary and non-deforming one. Since the mapping involves the random cylinder velocity, it is a random process itself and is also represented by a polynomial chaos expansion.

4.3. Numerical results

The Reynolds number is $Re = 100$, and the random parameters for the structure (see Eq. (13)) take the following form:

$$\begin{aligned} c &= \bar{c} + \sigma_c \xi_1(\theta), \\ k &= \bar{k} + \sigma_k \xi_2(\theta), \end{aligned} \tag{14}$$

where ξ_1 and ξ_2 are two independent random variables with zero mean, and σ_c and σ_k are the standard deviations of c and k.

We set $(\bar{c}, \sigma_c) = (0.1, 0.01)$, $(\bar{k}, \sigma_k) = (1.0, 0.2)$ while the initial conditions η_0 and $\dot{\eta}_0$ are set to 0. We note that there is a non-zero probability that the oscillator has a natural frequency $\omega_0 = \sqrt{k}$ matching the vortex shedding frequency of a fixed

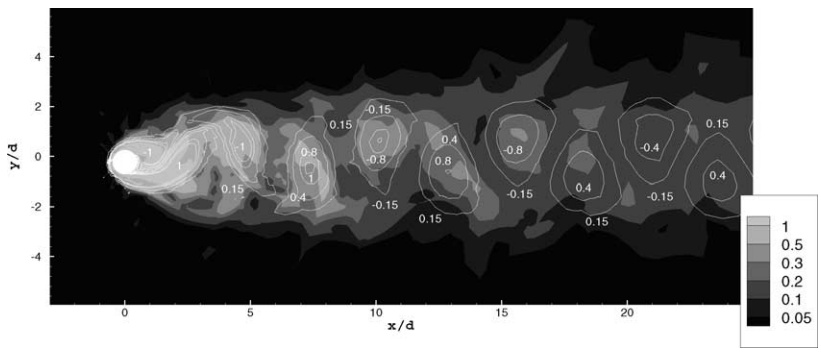

Fig. 5. Instantaneous spatial distribution of *rms* (gray scale) and *mean* (white line) of vorticity.

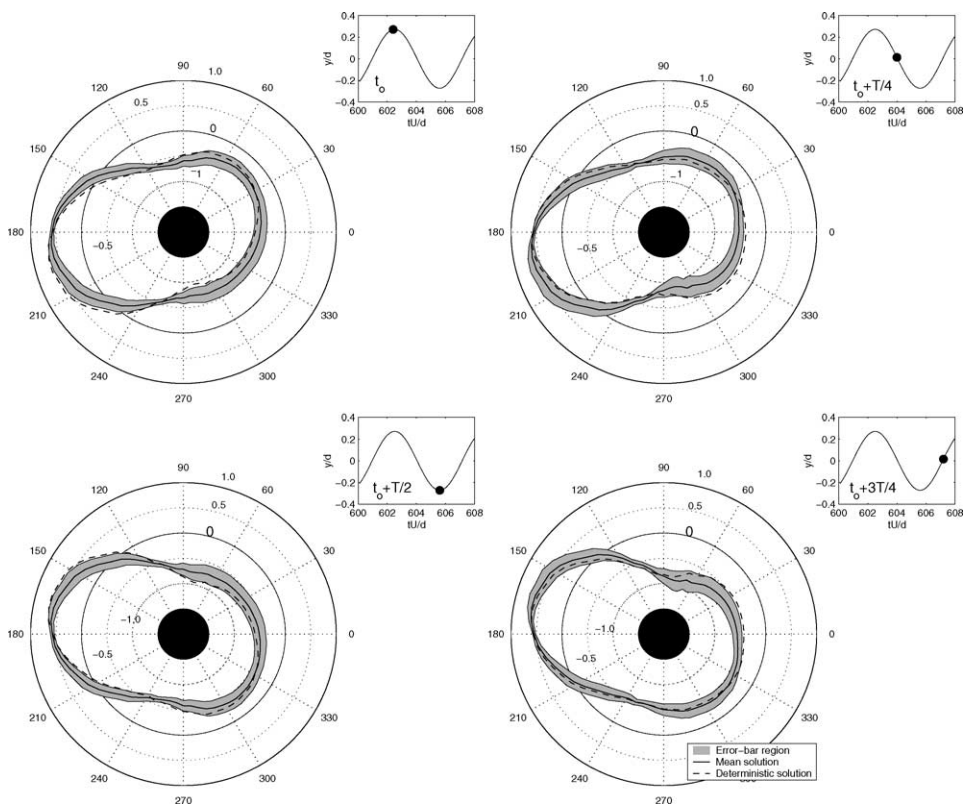

Fig. 6. Polar plots of pressure distribution on the cylinder surface relative to the cylinder *mean* cross-flow position at different times within one shedding cycle. Deterministic pressure solution (dashed line); stochastic pressure solution (solid line and shaded area).

cylinder at this Reynolds number. Also, the system has two random dimensions ($n = 2$), and we use third-order Polynomial Chaos expansion ($p = 3$), which corresponds to a 10-term chaos expansion (i.e., $P + 1 = 10$).

Mean and *variance* solution for the cross-flow displacement and lift and drag coefficients are obtained using this method. Fig. 5 shows instantaneous flood countours (gray scale) and countour lines (white color) of *rms* and *mean* of the vorticity field at $t = 600$ (non-dimensional time units, corresponding to more than 100 shedding cycles from the beginning of the simulation). Regions of the flow domain with high uncertainty are the shear layers and the near-wake of the cylinder, which are of course the regions of utmost physical interest!

Fig. 6 presents the pressure distribution on the cylinder surface at four instants of time within one shedding cycle of period T. Each plot shows an instantaneous polar view of the pressure distribution on the cylinder surface as well as the mean cross-flow position of the cylinder y/d at the corresponding time. The cylinder is represented by a black disk. The flow orientation is from left to right in each plot (angle $\theta = 180°$: front stagnation point and $\theta = 0°$: rear stagnation point). The deterministic pressure solution is represented by a dashed line while the stochastic solution is represented by a solid line (mean pressure solution) and a shaded area (‘*error−bar*’ region of the pressure solution). This region is centered around the mean curve and its span is two standard deviations (i.e., one *std* above and one *std* below the mean value). Both deterministic and stochastic pressure solutions take positive values around the front stagnation point. Noticeable differences exist between stochastic and deterministic solutions. In particular, temporal as well as spatial changes in the pressure variance (or ‘*error−bar*’ region) can be seen. However, the deterministic signal remains, most of the time, inside the envelope of the stochastic solution.

5. Conclusion

In this paper, we reviewed some of the main results and developments that we obtained using DNS as a tool for VIV predictions. We also presented a new path of research that addresses the issue of uncertainty in flow–structure interaction problems. We have addressed the effects of linear and exponential sheared flows in the context of VIV of long flexible cylinders. The ability of spectral DNS to accurately capture the resulting complex wake flows was demonstrated based on comparisons with experimental results.

We have developed algorithms for non-linear cables with variable tension. Specifically, we developed a unified formulation for non-linear cables in terms of a stretching parameter Δ for incompressible materials and area-preserving materials. This formulation was applied to the case of the flow induced by the motion of a very long and highly deformed riser in the ocean subject to a harmonic force at one of its ends.

We have also discussed the construction of error bars in CFD that reflect physical input uncertainty and its propagation in simulations. To this end, we used the Wiener–Hermite polynomial functionals that we applied to the two-dimensional flow–structure interaction case of an elastically mounted cylinder with uncertain structural properties. Representative results show that for flow–structure simulations, it is possible to quantify uncertainty both *in time* and *in space* efficiently.

Acknowledgements

We would like to thank the Office Of Naval Research for supporting this work (Dr. Thomas F. Swean). We are grateful to Prof. M.S. Triantafyllou for useful discussions related to this work. Computations were performed on the Cray T3E at ERDC (Engineer Research and Development Center) and on the IBM SP3 at MHPCC (Maui High Performance Computing Center).

References

[1] C. Evangelinos, G.E. Karniadakis, Dynamics and flow structures in the turbulent wake of rigid and flexible cylinders subject to vortex-induced vibrations, J. Fluid Mech. 400 (1999) 91–124.
[2] C. Evangelinos, D. Lucor, G.E. Karniadakis, DNS-derived force distribution on flexible cylinders subject to VIV, J. Fluids Structures 14 (2000) 429.
[3] D. Lucor, G.E. Karniadakis, Effects of oblique inflow in vortex induced vibrations, in: Proc. of IUTAM Symposium Unsteady Separated Flows, Toulouse, France, April 8–12, 2002.
[4] D.J. Newman, G.E. Karniadakis, Simulations of flow past a freely vibrating cable, J. Fluid Mech. 344 (1997).
[5] C. Evangelinos, Parallel simulations of VIV in turbulent flow: linear and non-linear models, Ph.D. thesis, Division of Applied Mathematics, Brown University, 1999.
[6] C.H.K. Williamson, Oblique and parallel modes of vortex shedding in the wake of a circular cylinder at low Reynolds numbers, J. Fluid Mech. 206 (1989) 579–627.

[7] D. Lucor, L. Imas, G.E. Karniadakis, Vortex dislocations and force distribution of long flexible cylinders subjected to sheared flows, J. Fluids Structures 15 (2001) 641–650.
[8] A.H. Techet, F.S. Hover, M.S. Triantafyllou, Vortical patterns behind a tapered cylinder oscillating transversely to a uniform flow, J. Fluid Mech. 363 (1998) 79–96.
[9] M.S. Triantafyllou, G.S. Triantafyllou, D. Tein, B.D. Ambrose, Pragmatic riser VIV analysis, Technical report, Offshore Technology Conference, OTC 10931, 1999.
[10] C. Evangelinos, D. Lucor, C.-H. Su, G.E. Karniadakis, Flow-induced vibrations of non-linear cables. Part 1: Models and algorithms, Int. J. Numer. Methods Engrg. 55 (2002) 535–556.
[11] D. Lucor, C. Evangelinos, L. Imas, G.E. Karniadakis, Flow-induced vibrations of non-linear cables. Part 2: Simulations, Int. J. Numer. Methods Engrg. 55 (2002) 557–571.
[12] T.C.E. Warburton, Spectral/hp element methods on polymorphic multi-domains: algorithms and applications, Ph.D. thesis, Division of Applied Mathematics, Brown University, 1998.
[13] D. Xiu, D. Lucor, C.-H. Su, G.E. Karniadakis, Stochastic modeling of flow-structure interactions using generalized polynomial chaos, J. Fluid Engrg. 124 (2002) 51–59.
[14] D. Lucor, Generalized polynomial chaos: applications to random oscillators and flow–structure interactions, Ph.D. thesis, Brown University, in preparation.